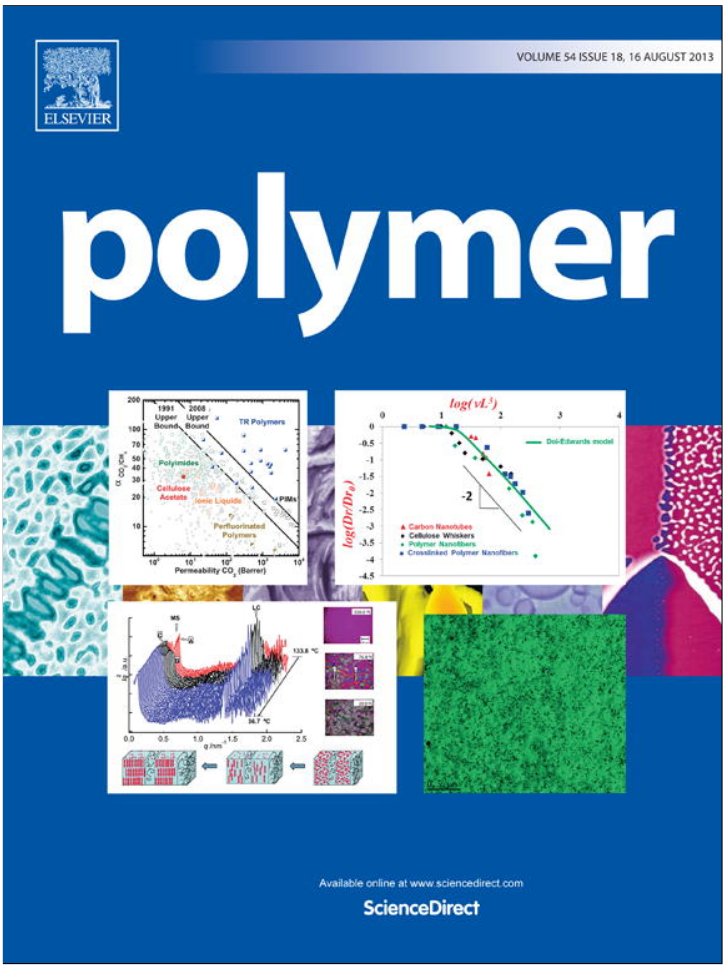

Polymer 54 (2013) 5064–5074

Contents lists available at SciVerse ScienceDirect

Polymer

journal homepage: www.elsevier.com/locate/polymer

A molecular dynamics study of tensile strength between a highly-crosslinked epoxy molding compound and a copper substrate

Shaorui Yang [a], Feng Gao [b], Jianmin Qu [a,b,*]

[a] Department of Mechanical Engineering, Northwestern University, 2145 Sheridan Rd, Evanston, IL 60208, USA
[b] Department of Civil and Environmental Engineering, Northwestern University, 2145 Sheridan Rd, Evanston, IL 60208, USA

ARTICLE INFO

Article history:
Received 3 May 2013
Received in revised form
22 June 2013
Accepted 3 July 2013
Available online 11 July 2013

Keywords:
Epoxy molding compound
Copper substrate
Molecular dynamics simulation

ABSTRACT

Presented in this paper is a numerical study based on classical molecular dynamics simulation to understand the deformation and failure behavior of an epoxy/copper bimaterial under pure tension normal to the interface. The epoxy considered is a highly cross-linked epoxy phenol novolac, and the copper substrate is a standard face-center-cubic single crystal with its (1,1,1) surface as the epoxy/copper interface. Stress versus displacement/strain curves are obtained to understand the bimaterial behavior and to predict the epoxy/copper interfacial tensile strength. It is found that the interfacial failure is brittle caused by simultaneous detachment of epoxy atoms from the copper substrate, and the interfacial tensile strength is almost unaffected by the unloading and reloading before the failure strength is reached. Effects of temperature, epoxy cross-link density, and epoxy functionality are also investigated. Findings of this study provide significant insights into the deformation and failure behavior mechanisms of the epoxy/copper bimaterial interface.

1. Introduction

Bimaterial interfaces are common in electronic packages, most of which have large mismatch in material properties such as elastic constants and thermal expansion coefficient. Among the various bimaterials of engineering interest, interfaces between epoxy molding compound (EMC) and copper (Cu) are probably the most prevalent ones. Because EMC/Cu interfaces are the weakest links and prone to delamination, they are considered critical to the reliability of electronic devices. Traditional methodologies of characterizing the interface's performance involves extensive destructive tests, such as fracture of sandwiched double-cantilever beam [1,2] and peeling-off of thin film bonded by epoxy adhesive to solid substrates [3]. However, experimental tests are typically time/recourse consuming. More importantly, they are often incapable of revealing the microstructure of the polymer network near the interface and how the microstructure affects the mechanical properties. On the other hand, molecular dynamics (MD) simulations are capable of describing material behavior at atomistic level and thus providing insights into the structure-property relationship. We present here an MD study of highly-crosslinked epoxy resin bonded to a copper substrate. Using MD simulation, we are able to precisely control the structural and loading parameters and study their influence on the traction-displacement/strain behavior of the interface system. In fact, it has been extensively applied to study interfacial deformation/failure behavior between crystalline solids [4–7].

Probably because of the complexity of epoxy's atomistic structure, very few molecular simulations of epoxy have been reported. Atomistic models for epoxy resins and general polymer networks have been constructed based on molecular dynamics simulation of polymerization [8–14]. Several MD studies of bulk epoxies based on these type of models have been performed focusing on predicting/reproducing the material's thermal [8,10,11,15–17], dynamic [18–20] and mechanical [8,12,15–17,21] properties. These MD simulation results show good agreement with experimental measured values, indicating the validity of the methodology of building polymer networks.

In contrast to bulk materials, there are very few publications using MD simulations to study the interfaces between epoxy molding compounds and in-organics substrates. Stevens et al. [22–24] and Mukherji and Abrams [25,26] investigated deformation/failure behavior of highly-crosslinked polymer network constrained by crystalline substrates, based on coarse-grained model and potentials. These studies are for model material systems and the results are not in physical dimensions because of their use of

* Corresponding author. Department of Civil and Environmental Engineering, Northwestern University, 2145 Sheridan Rd, Evanston, IL 60208, USA. Tel.: +1 847 467 4528.
E-mail addresses: yangshaoruigt@gmail.com (S. Yang), j-qu@northwestern.edu (J. Qu).

0032-3861/$ – see front matter © 2013 Elsevier Ltd. All rights reserved.
http://dx.doi.org/10.1016/j.polymer.2013.07.019

coarse-grained approach. In the literature, full-atomic MD simulations have been used to study epoxy/substrate bimaterials. For example, Jia et al. [27] and Cheng et al. [28] studied interfacial energy and bonding strength between epoxy and self-assembly-monolayer coated Au surface using MD simulations. The most relevant work to the present study is the MD simulation of the DGEBA-MDA epoxy/Cu bimaterial using the COMPASS force-field [29]. Besides simulating only a very small material volume (3.53×3.53 nm^2 in the x and y direction and a few thousand atoms), much of the epoxy network in their study is assumed rigid except atoms very close to the interface. As will be seen from our studies, such assumptions may not be appropriate for obtaining the strength or toughness of the interface due to the longer-range nature of the atomistic interaction in the epoxy network.

In order to investigate the deformation and failure behavior of the highly crosslinked epoxy/Cu interfaces, we carried out large scale MD simulations on an epoxy/Cu bimaterial. The epoxy/Cu bimaterial is made of a highly-crosslinked epoxy molding compound attached to a Cu substrate. The network structure of the epoxy was constructed through a simulated crosslinking process in which covalent bonds formation and MD equilibration of the system were performed iteratively. The crosslinked molecular network was applied on the Cu substrate to form the epoxy/Cu bimaterial. By applying velocity loading to the substrate during the MD simulation, the normal stress versus displacement/strain response was obtained. Effects of simulation cell size were studied to ensure that the results are independent of simulation cell size. In addition to the stress–strain relationship, we also investigated the effects of cyclic loading, temperature, conversion and epoxy monomer functionality on the stress–strain relationship. The rest of the paper is organized as follows. In Section II, the atomistic model and the loading set-up are presented. Simulation results and influence of various structural and loading parameters are discussed in Section III. Finally, some conclusion remarks are summarized in Section IV.

To close this section, we note that the methodology developed here for modeling the epoxy modeling compound/Cu bimaterial is not restricted to the specific epoxy formulation in the current work, but can be extended to various other epoxy systems. Therefore, results from this study provide guidance to designing polymer/metal interfaces in the electronic packaging industry.

2. Simulation method

2.1. Material system and MD simulation cell

For this study, a commercially important epoxy system, Epoxy Phenol Novolac (EPN) is chosen. The polymer is based on using EPN1180 as the epoxy and Bisphenol-A (BPA) as the hardener [30]. Their molecular structures are shown in Fig. 1(a). The epoxy monomer is a mixture of 3mers and 4mers, and the number-averaged functionality is 3.6. The mechanism of the crosslinking reaction is illustrated in Fig. 1(b) and is explained in detail elsewhere [17].

The atomistic model for the epoxy system was created from a mixture of EPN1180 and BPA monomers. First, an orthogonal simulation cell of dimension $W \times D \times H$ was constructed using the Amorphous Cell module in the Material Studio software [31]. Next, the EPN1180 and BPA monomers were randomly seeded within the simulation cell with confined layer geometry constructed following the self-avoiding random walk method of Theodorou and Suter [32]. The number of monomers used follows the ratio of 2:3:9 among the tri- and tetra-functionalized epoxies and hardeners. Finally, the polymer cell is placed on the (1,1,1) surface of a single crystal copper (Cu) substrate of dimension $W \times D \times h$. This forms an epoxy/Cu bimaterial, see Fig. 2. For convenience, a Cartesian coordinate system is attached to the bimaterial, where the x-axis and the y-axis are in the epoxy/Cu interface and the z-axis is perpendicular to the interface.

2.2. Interatomic potentials

In our MD simulations, interactions between the atoms in the polymers are described by an extensively parameterized and validated force-field, the Polymer Consistent Force-Field (PCFF) [33–36] given below,

$$
\begin{aligned}
E_{\text{total}} = {} & \sum_b \left[k_2(b-b_0)^2 + k_3(b-b_0)^3 + k_4(b-b_0)^4\right] + \sum_\theta \left[H_2(\theta-\theta_0)^2 + H_3(\theta-\theta_0)^3 + H_4(\theta-\theta_0)^4\right] \\
& + \sum_\varphi [V_1(1-\cos\varphi) + V_2(1-\cos 2\varphi) + V_3(1-\cos 3\varphi)] + \sum_\chi K_\chi \chi^2 \\
& + \sum_{b,b'} F_{bb'}(b-b_0)\left(b'-b_0'\right) + \sum_{b,\theta} F_{b\theta}(b-b_0)(\theta-\theta_0) + \sum_{\theta,\theta'} F_{\theta\theta'}(\theta-\theta_0)\left(\theta'-\theta_0'\right) \\
& + \sum_{b,\varphi}(b-b_0)(V\cos\varphi + V_2\cos 2\varphi + V_3\cos 3\varphi) + \sum_{\theta,\varphi}(\theta-\theta_0)(V\cos\varphi + V_2\cos 2\varphi + V_3\cos 3\varphi) \\
& + \sum_{b,\theta,\varphi} F_{b\theta\varphi}(b-b_0)(\theta-\theta_0)\cos\varphi + \sum_{i,j}\frac{q_i q_j}{r_{ij}} + \sum_{i,j}\varepsilon_{ij}\left[\frac{A_{ij}}{r_{ij}^9} - \frac{B_{ij}}{r_{ij}^6}\right]
\end{aligned}
\tag{1}
$$

The PCFF consists of both valence and non-bond terms. Valence terms include interactions due to bond, angle, dihedral and improper, as well as coupling between them. Non-bond terms are the Coulombic forces between partially charged atoms and the Lennard-Jones (LJ) 9-6 potential representing the van der Waals forces. In the examples presented in this paper, the LJ potentials and the real-space contribution to the Coulombic energy were calculated with a cut-off distance of 12.5Å. The Coulombic term's reciprocal-space contribution was computed by the particle-particle-particle-mesh method.

Since the deformation in the Cu substrate is negligible, we assumed that the Cu substrate is rigid. Further, it is reasonable to assume [37] that the epoxy is bonded to the Cu substrate through van der Waals forces only (no covalent bond). Thus, the interaction between the polymer atoms and Cu atoms can be described by the LJ 9-6 potential whose parameter are obtained from the parameters of copper and epoxy atoms following the sixth-power mixing law [38],

$$
\varepsilon_{ew} = \frac{2\sigma_e^3\sigma_w^3\sqrt{\varepsilon_e\varepsilon_w}}{\sigma_e^6+\sigma_w^6}, \quad \sigma_{ew} = \left(\frac{\sigma_e^6+\sigma_w^6}{2}\right)^{1/6} \tag{2}
$$

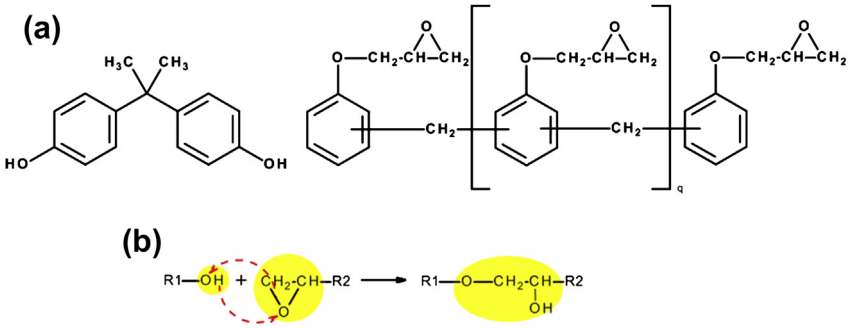

Fig. 1. (a) Molecular structure of BPA (left) and EPN (Right); (b) Curing reaction mechanism [30].

where the subscripts *e* and *w* stand for epoxy and copper substrate, respectively.

2.3. Construction of the polymer network

To simulate the crosslinking of the polymer, boundary conditions were prescribed so that the simulation cell is periodic in the plane of the epoxy/Cu interface, and traction-free in the direction normal to the interface. Under these boundary conditions, mixture of monomers was dynamically crosslinked into a network using a script [17] running in the Material Studio software. During this crosslinking process, chemical bonds were formed between a pair of opposite reactive atoms, namely the ending epoxy carbons on resins and the hydroxyl oxygen on hardeners, provided that they were within a prescribed cut-off distance. After all such reactive atoms were bonded, the system was equilibrated by 1000 steps of energy minimization and 10,000 steps of NVT MD simulation at 500 K to release internal stress caused by the newly formed bonds and bring remaining reactive atom pairs into proximity. This crosslinking-equilibration process proceeded repeatedly until a desired conversion is achieved. To speed up the process, the bond formation cut-off distance was increased from 3 to 10Å incrementally. At each cut-off, five crosslinking-equilibration loops were conducted. After reaching the desired conversion, the un-reacted reactive sites were saturated with hydrogen atoms and partial charges to make the entire system charge neutral. Due to the periodic boundary conditions in the plane of the interface, covalent bonds formed not only between the monomers inside the simulation cell, but also between monomers and their virtual images across the periodic boundaries. Therefore, the polymer network percolates to infinity in the plane of the interface. Finally, MD simulations were conducted to minimize the system energy and to equilibrate the atomistic structure under traction-free conductions. More detailed discussion of this computational algorithm to simulate crosslinking can be found in Ref. [17].

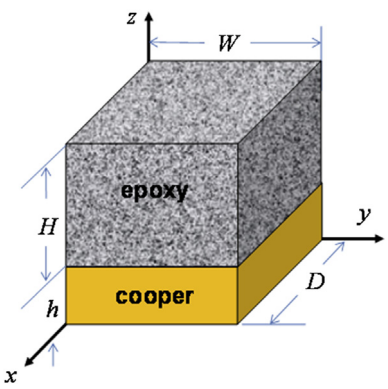

Fig. 2. Schematic of the epoxy/Cu bi-material.

2.4. Tensile simulation

To conduct simulation of uniaxial deformation of the epoxy/Cu bimaterial system, the very top layers of the polymer atoms are fixed, see Fig. 2. The Cu substrate is assumed to be a rigid body moving downward with a prescribed velocity. A constant NVT MD simulation was conducted at 300 K with the timestep of 1 fs using the LAMMPS software [39]. The Nose-Hoover thermostat was applied to control the system's temperature. The virial stress tensor in the epoxy was calculated and outputted as a function of the total elongation of the epoxy/Cu bimaterial.

3. Results and discussions

3.1. Effects of the simulation cell size and strain rates

We need to use a simulation cell that is large enough so that the results are independent of the cell size. To this end, three simulation cells of different sizes were considered, see Table 1. It was found that the overall stress–strain relationship for cell #1 changes significantly with the initial configuration before crosslinking, which indicates that the in-plane dimension is not large enough to generate unique mechanical behavior. The two bigger cells do not suffer from this problem. The normal stress in the *z*-direction versus its corresponding strain for cells #2 and #3 are plotted in Fig. 3. It is seen from Fig. 3 that the stress–strain curve does not change much after doubling the cell size, indicating that the size of cell #2 is sufficient to study the normal stress versus strain behavior. Thus, cell #2 will be used in the rest of this article.

We note that, in the above simulations, the prescribed velocity of the Cu substrate is 5×10^{-5} Å/fs for cell #2, which corresponds to a strain rate of $\sim 5 \times 10^{8}$ s^{-1}. The same strain rate was used in cell #3. The strain rate's effect on stress-strain behavior was investigated by applying three different rates to cell #2, and their results are shown in Fig. 4. Stress–strain curves are very close among these three rates and the failure property does not show clear trend with respect to strain rate. Therefore we will use the rate 5×10^{8} s^{-1}

Table 1
Dimensions of the simulation cells.

No.	Number of atoms	$W \times D$ (Å^2)	H (Å)
1	24,194	44.48 × 44.48	110
2	96,776	88.96 × 88.96	110
3	179,552	88.96 × 88.96	220

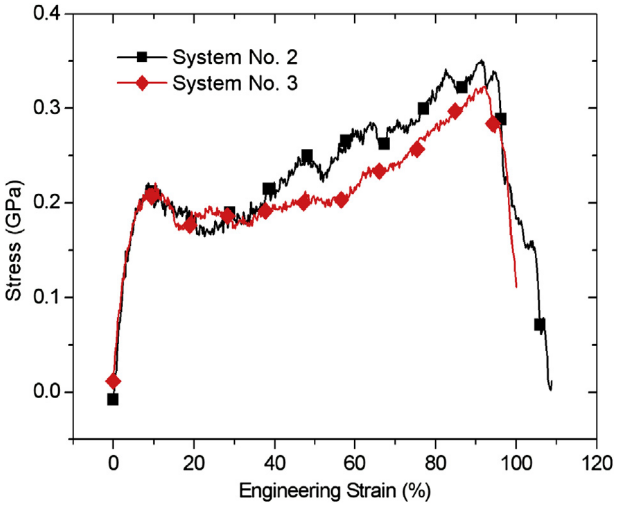

Fig. 3. Stress versus strains curves for cells #2 and #3.

throughout the rest of this article. This strain rate is obviously much higher than that used in quasi-static loading in realistic laboratory tests. Therefore, results given in the remainder of this paper must be interpreted with this high strain rate in mind.

3.2. Deformation behavior

It is seen from Fig. 3 that stress–strain relationship is almost linear initially until the yielding strength of 0.22 GPa is reached at the strain of ~8.7%. Regarding the variation of the system's potential energy, Fig. 5(a) shows that the total and non-bond potential energies both increase with strain, while Fig. 5(b) shows slight decreases of bonding, angular and torsional energies within the elastic regime. This implies that the initial configuration represents a state in which valence degrees of freedom are constrained. Upon loading, constraints imposed on bonds, angles and torsions are released and so are their corresponding stored potential energies.

Fig. 6 shows snapshots of simulation cell #2 at different stages of the deformation. The first snapshot in the row is at yielding, in which no visible damage is observed. The post yielding behavior is characterized by strain softening from the yielding strength to 0.16 GPa, followed by strain hardening extending to the ultimate

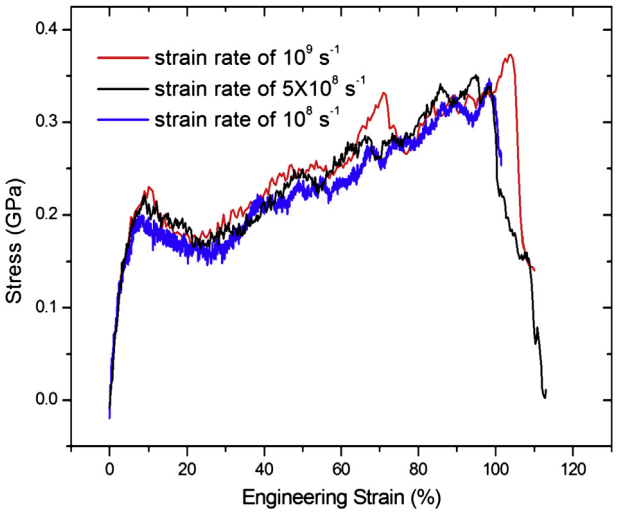

Fig. 4. Stress versus strains curves for cells #2 using different strain rates.

interfacial failure. At this stage, it is seen from the second snapshot that micro-voids are initiated in regions of the polymer network with lower connectivity, due to the tri-axial stress state within the epoxy layer. The tri-axial stress state is consistent with the zero in-plane strain condition in realistic adhesive layers which are highly constrained by adherends [40,41].

These micro-voids enlarge and coalesce as the tensile deformation proceeds, as is shown in the third snapshot. At the meantime, polymer chains are being pulled taut from their initial configuration. This process, we argue, is accomplished via angle bending and dihedral torsion instead of direct bond stretching, because, as shown in Fig. 5(b), the bond energy experiences negligible post-yielding change, while the angular and torsional energy show significantly more drastic changes. The increase of angular energy is due to the change of angles. The decrease in torsional energy indicates that the dihedrals were not in their equilibrium states, and tensile deformation moves them back to their equilibrium states.

At ~95% strain, the normal stress reaches the failure strength of approximately 0.34 GPa and drops abruptly to zero. It is seen from the last snapshot in Fig. 6 that failure is the result of debonding of the epoxy from the Cu substrate. Our simulations also show that immediately after the interfacial failure, the epoxy recoils back. Accordingly, angular/torsional energy drastically decreases/increases after reaching their maximum/minimum, as can been seen in Fig. 5(b).

3.3. Bulk versus interfacial deformation

The strain in the stress–strain curves shown in Fig. 3 consists of the deformation occurred in the bulk of the epoxy and in the epoxy/Cu interface (the Cu substrate is assumed rigid). The bulk epoxy deformation is governed by the PCFF given in Eq. (1), and the interaction across the epoxy/Cu interface is the van der Waals force described by the LJ 9-6 potential given in Eq. (2). The potential well depth of copper is typically one or two orders of magnitude larger than that of epoxy atoms. Therefore, the van der Waals forces across the interface are strong attractions. Furthermore, the initial epoxy network is a fully relaxed one. Thus, at lower strain level, the bulk epoxy deforms relatively easily through the rearrangement of the polymer network (angles and torsion). Consequently, bulk deformation is predominant. However, since the epoxy has a highly constrained network microstructure, there is a limit for the rearrangement of strands to accommodate the deformation. Beyond that, valence forces within the polymer kick in. The bulk epoxy becomes significantly stiffer than the van der Waals interaction at the epoxy/Cu interface. Thus, at higher strain level, the deformation occurring at the epoxy/Cu interface becomes non-negligible, which eventually fails the interface.

To demonstrate the above analysis, a numerical experiment was conducted, in which the bulk epoxy (with the Cu substrate removed) was subjected to tensile deformation by applying the same downward velocity to the bottom of the bulk epoxy as if the Cu substrate were present. The corresponding stress–strain curve is plotted in Fig. 7 together with that of the epoxy/Cu bimaterial. It is seen that these two curves are almost identical at lower strain level (<46%). At higher strain level (>46%), they start to deviate. The difference between these two curves is due to the compliance of the interface. Another way of looking at this figure is by drawing a straight line of constant stress. Under the same stress, the bulk epoxy has smaller strain than the epoxy/Cu bimaterial. The additional strain in the epoxy/Cu bimaterial comes from the epoxy/Cu interface.

The large bulk deformation of the epoxy slab seems to contradict the brittle nature of epoxy observed in macroscopic

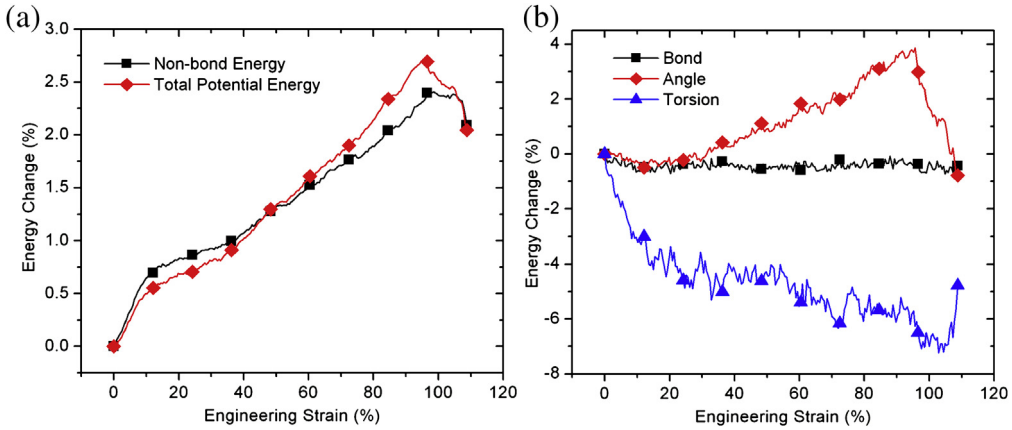

Fig. 5. Variation of (a) total and non-bond, and (b) valence potential energies with respect to strain.

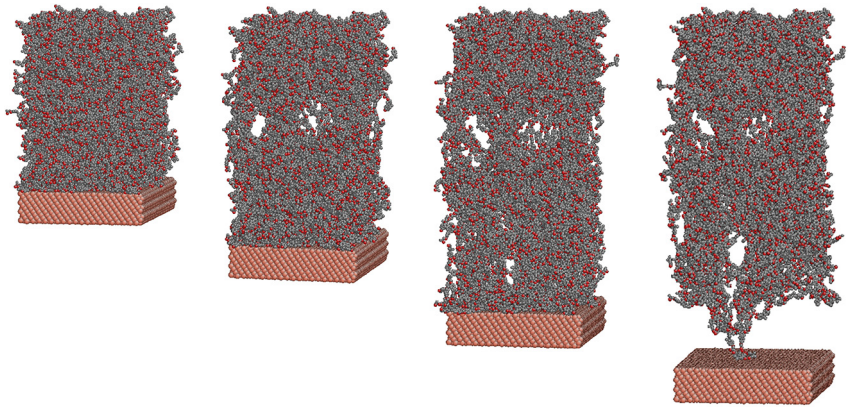

Fig. 6. Snapshots of atomic configurations during the tensile simulation. The different figures in a row represent strains (from left to right): 8.7%, 38.5%, 77.1% and 107.9%.

mechanical tests. This contradiction can be explained by the different length scales of observation used. In comparison with the laboratory test samples, the material volume simulated in this study is extremely small. The deformation observed is, therefore, extremely localized. Such localized large deformation has been observed experimentally, such as in crazes [42], dilatation bands [43] and shear bands [44,45]. Regarding interfaces, local plastic deformation has been observed as ridges on epoxy fractured surface from glass [46] and sapphire [47] substrates.

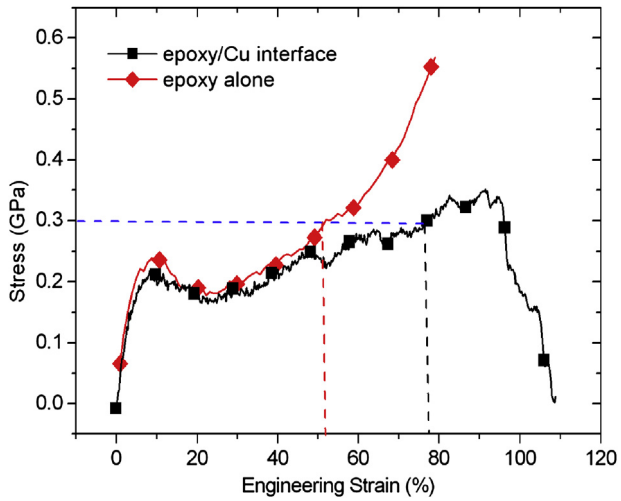

Fig. 7. Stress–strain curves for the epoxy/Cu interface and the epoxy slab alone, respectively.

The interfacial failure strength in our MD simulation is 340 MPa, higher than experimental measured values ranging from ~50 MPa for epoxy/steel [48,49] to 120 MPa for epoxy/bare-sapphire [47]. However, it is known that MD simulated local stresses could be much higher than macroscopically measured stress in typical laboratory test samples. For example, Gall et al. [4] reported the debonding strength of Al–Si bimaterial to be 20 GPa, which contrasted sharply with the experimental measured ultimate tensile strength (~200 MPa) of cast Al–Si alloy [50,51]. In our case, the deformation within the MD simulated region is all due to the stretching of discrete molecular fibrils. Therefore, stress magnitude could be much higher. In fact, some analysis [23] of the self-assembled monolayer (SAM) revealed that the separation strength of two methyl-terminated alkylsiloxane SAM coated surfaces, which is solely due to van der Waals interaction, could be as high as 320 MPa. This class of interactions (SAM–SAM) corresponds to those involved in epoxy bonded to silicon oxide substrate [23]. Therefore, our computed strength of 340 MPa is reasonable as far as separation of atomic surfaces is concerned. Clearly, more work is needed in order to use the MD results in macroscopic samples.

3.4. Unloading and reloading behavior

To understand how the bimaterial behaves under cyclic loading (loading-unloading-reloading), molecular dynamics

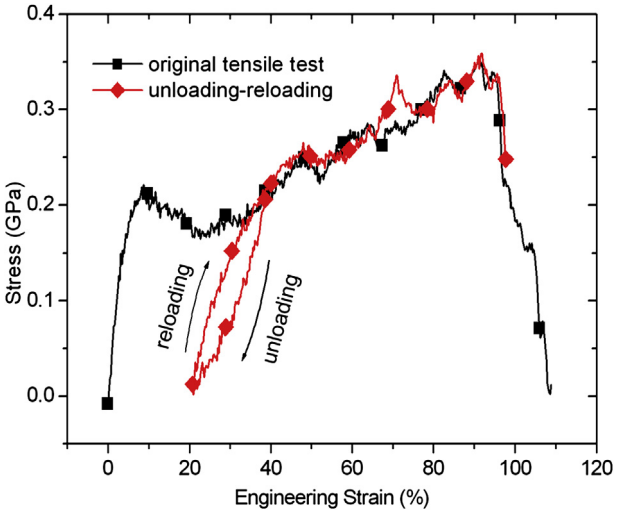

Fig. 8. Unloading-reloading behavior of the epoxy/Cu interface system.

simulations were conducted. First, a simulation cell was subjected to tensile loading up to the strain of 38.5%. The bimaterial is then unloaded by reducing the applied tensile deformation following the same rate of deformation as for the original tensile test. As shown in Fig. 8, a residual strain of ~21% remains after the tensile load is completely removed (zero-\tensile stress). In the fully unloaded bimaterial (snapshot not shown here), irreversible damages are seen in the epoxy slab as voids. Accordingly, the non-bond potential energy fails to restore to its original value, see Fig. 9(a). By reloading the system, the stress–strain response forms a hysteresis loop with that of the unloading process. The area encompassed by the loop corresponds to the energy dissipation during the strain cycle, indicating a viscoplastic nature of the material's post yielding constitutive behavior. Fig. 9(a) and (b) demonstrate that the non-bond energy's reloading curve is lower than the unloading curve, while for angular and torsional energies the two coincide. This implies that the energy dissipation in the unloading-reloading cycle is associated with the polymer chains' translational motion, rather than the changes of intra-chain rotational degrees of freedom, i.e., angle bending and dihedral torsion. Reloading of the interface system attains the same failure strength/strain as the original tensile test, which is expected since the failure is solely controlled by the copper-epoxy inter-atomic potentials. This also indicates that the interface deforms elastically and is not damaged until the ultimate failure occurs.

3.5. Effects of temperature

To study the effects of temperature, MD simulations were conducted at several temperatures, $T = 340$, 380, 440 and 500 K. The resulted stress–strain curves are shown in Fig. 10, and the corresponding yielding and failure strengths are shown in Fig. 11. As expected, both the yielding and the failure strengths decrease with increasing temperature. In addition, there is a slight decrease in the yielding and failure strains as well. Note that, as discussed earlier, the yielding strength is predominately the bulk epoxy behavior, while the failure strength is the epoxy/Cu interface property. Therefore, the results shown in Fig. 10 indicate that temperature affects both the bulk epoxy and the epoxy/Cu interface. In bulk epoxy, yielding is caused by the change in angular and torsional bonds facilitated by the relative sliding among the polymer chains. Higher temperature lowers the activation energy and makes the sliding easier, thus reducing the yielding strength, as well as the modulus [17]. The interface, on the other hand is mainly associated with the inter-atomic forces at the interface between epoxy and Cu atoms, governed by the LJ potential. At higher temperature, the increased mobility of near-surface polymer strands lowers the energy consumption to break interfacial (non-covalent) bonds. Thus the failure strength reduces.

3.6. Effects of conversion

The conversion, or the fraction of reactive sites that have been reacted, significantly influences the mechanical properties such as the Young's modulus of bulk epoxy [17]. All the results presented in the previous sections are for the case of 95% conversion. In this section, we are interested in how the conversion affects the epoxy/Cu interfacial strength.

As crosslinking proceeds, the polymer's microstructure experiences a transition from liquid mixture of monomers to loosely connected fragments, and to highly constrained network. Each of the three phases exhibits different mechanisms of deformation and failure when loaded. To investigate the effect of conversion, three additional bimaterials with different epoxy conversions, $c = 50\%$, 73% and 82% were constructed and were subjected to the same MD simulation of tensile deformation as described in previous sections. Fig. 12 plots the stress versus strain curves for all four bimaterials. Prior to the occurrence of yielding, the four bimaterials exhibit similar elastic responses, indicating that the conversion does not

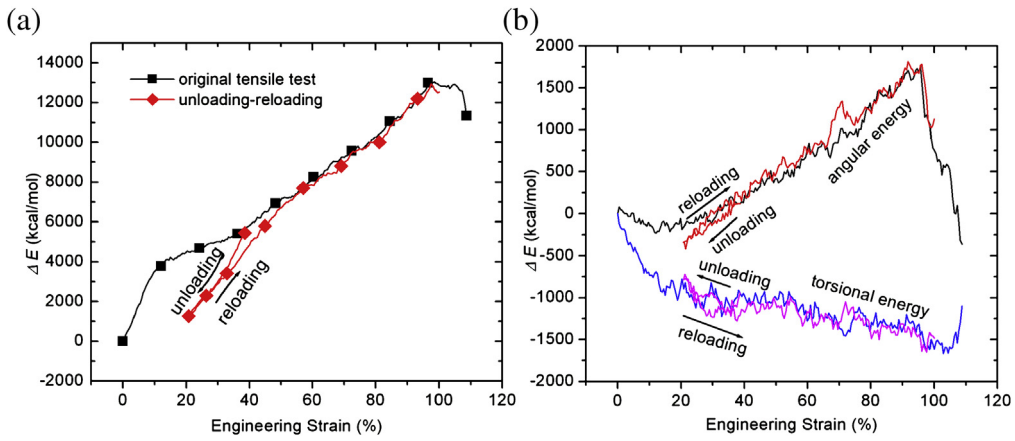

Fig. 9. Variation of the (a) non-bond and (b) valence potential energy components during the unloading-reloading process.

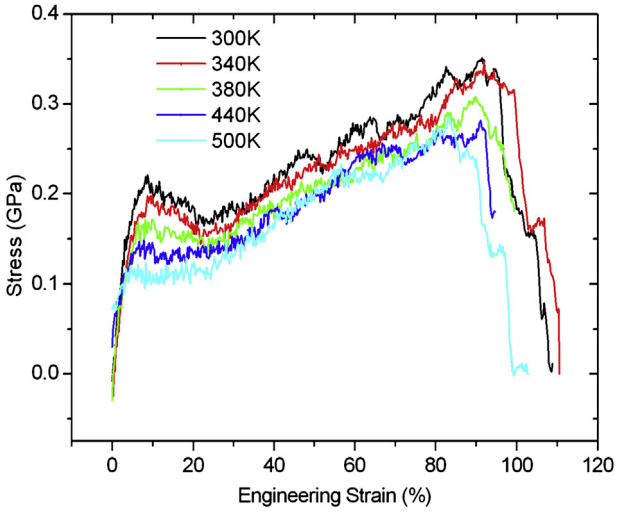

Fig. 10. Stress–strain curves at different temperatures.

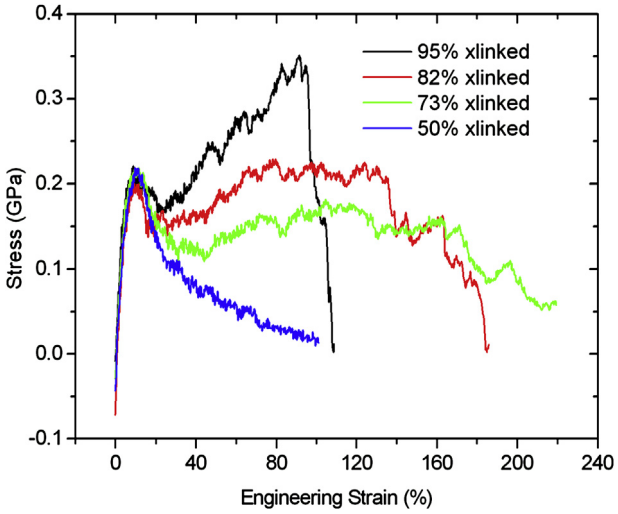

Fig. 12. Stress–strain curves for bimaterials with different epoxy conversions.

affect the linear elastic behavior. However, the post-yielding behavior is strongly affected by the conversion. For the least crosslinked (50%) system, strain-softening occurs immediately after yielding, and the tensile stress decreases to zero almost exponentially. Snapshots of the atomic configuration shown in Fig. 13(a) indicate that failure initiates within the epoxy in the vicinity of interface, and progresses as the tensile load increases. Following Miller and Macosko's method [52], the theoretical gelation point of our particular epoxy formulation (E3 + E4 + H2, E for epoxy and H for hardener, number stands for functionality) is 62%. Since a conversion of 50% is lower than the gelation point, the atomistic model of epoxy comprised many loosely connected molecular fragments rather than a system-spanning cluster. Therefore, the presence of a thin layer of molecules near the interface, which lacks sufficient covalent links to the epoxy bulk, is likely. Failure of the interface system is thus seen as the cohesive separation between this thin layer and the rest portion of epoxy. Fibrils vertically bridging the two parts are present at intermediate strains, but bounce back to epoxy bulk and return to coiled state as tensile deformation continuously proceeds. On the other hand, the thin layer in the vicinity of interface would remain attached to the substrate.

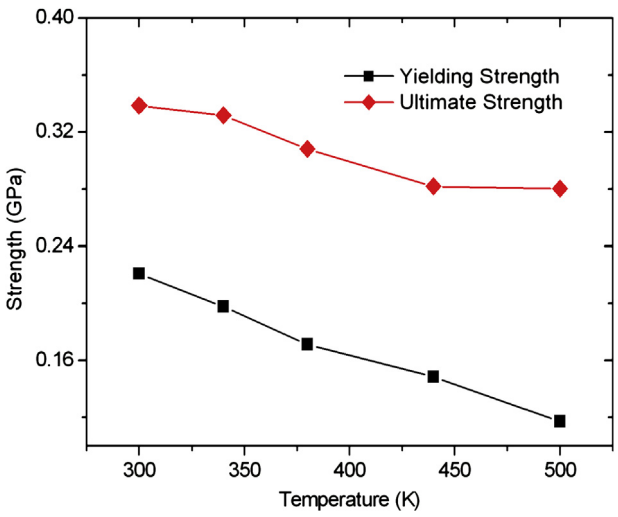

Fig. 11. Yield and failure strengths of the bimaterial versus temperature.

The systems with conversions of 73% and 82% exhibit deformation behaviors which are intermediate between extreme cases. For both bimaterials, the tensile stress decreases after reaching the yielding point and experiences strain hardening regime, followed by stress plateau until failure (green and red curves in Fig. 12). Magnitudes of their post-yielding stress are lower than that of the 95% conversion. The reason lies in the fact that lower conversion facilitates more micro-voids to initiate, grow and coalesce, which can be evidenced by the larger average void size in the post-yielding atomic configurations shown in Fig. 13(b). The higher level of damage to the bulk epoxy leads to more drastic stress drop after yield.

In these lower conversion bimaterials, the ultimate failure occurs at larger strains but lower strengths, both can be attributed to the difference in microstructure. At lower conversions, the polymer chain network is less connected. This results in more not-crosslinked polymer strands in the epoxy. When deformed, these strands require larger overall strain to be stretched taut from their coiled state. Thus the failure strain is extended.

As discussed in previous sections, the failure strength of the bimaterial is related to the epoxy/Cu interface. Snapshots of the atomic configuration, see Fig. 6, indicate that interfacial failure is caused by the simultaneous separation of all polymer atoms from the Cu substrate that results in the brittle failure shown by the stress–strain curve, see Fig. 12. It is also seen from Fig. 12, that bimaterials with lower conversions, on the other hand, show a more ductile failure behavior. This ductile behavior is due to the gradual peeling-off of polymer chains from the Cu substrate, as observed in the snapshots shown in Fig. 13(b). Such gradual detachment of polymer chains from the Cu substrate decreases the interfacial strength, and increases the failure strain. To quantify this observation, we plotted in Fig. 14 the number of epoxy atoms in the vicinity (van der Walls cutoff distance) of the epoxy/Cu interface as a function of tensile deformation. It is clear that lower conversion leads to more gradual interfacial separation of epoxy atoms from the Cu substrate.

Table 2 summarizes the failure strength and strain for different bimaterials. From 73% to 95%, strength and strain increases and decreases, respectively, with increasing conversion. The bimaterial with conversion of 50% (below the gelation point), fails cohesively instead of interfacially, thus needs to be interpreted separately.

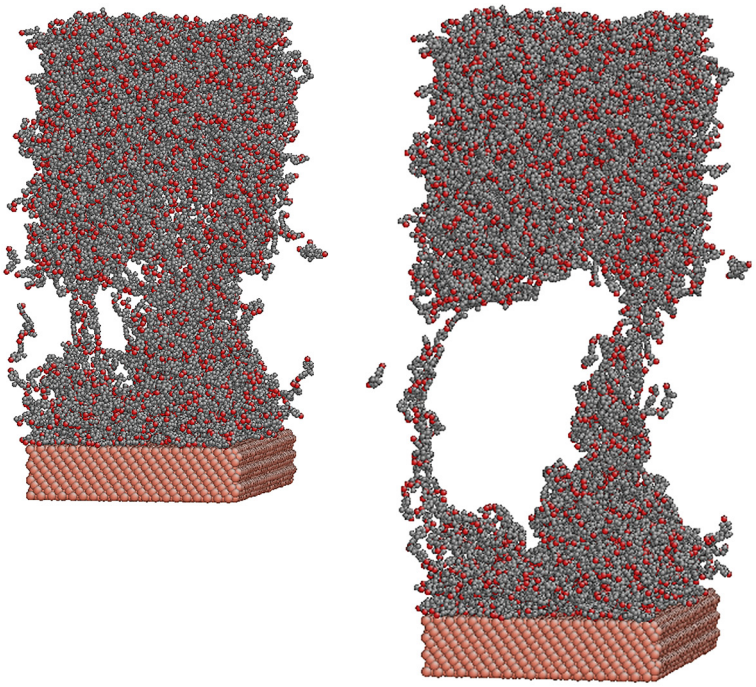

(a)

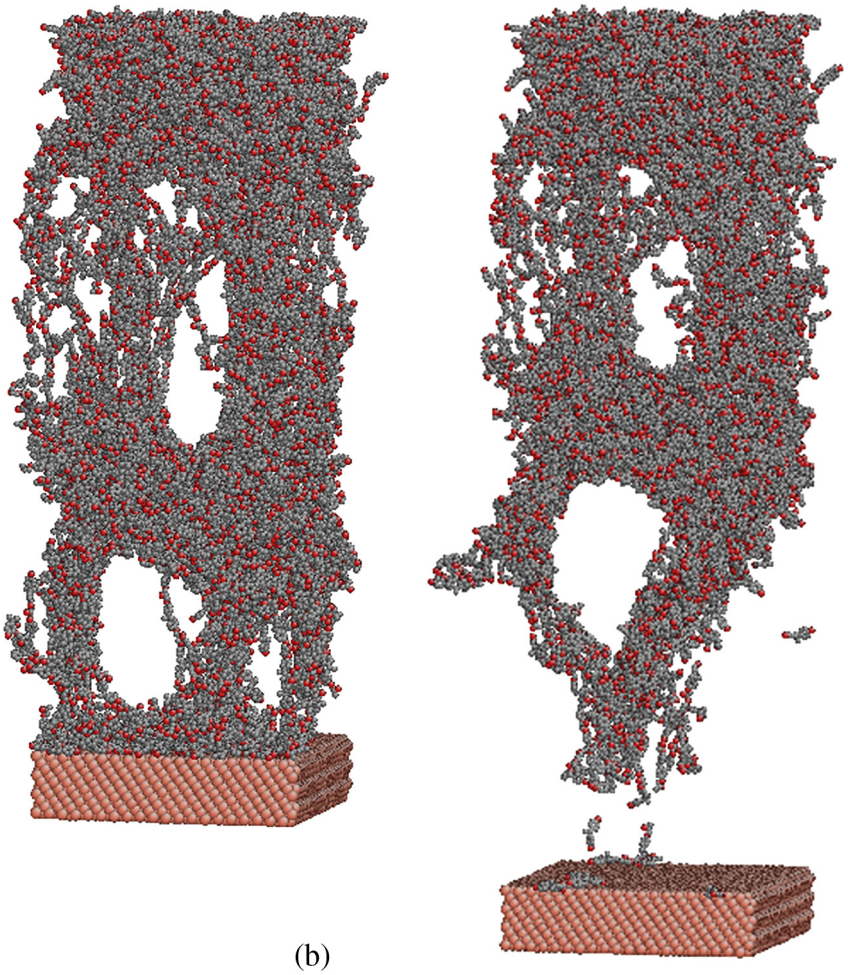

(b)

Fig. 13. Atomistic configurations during tensile deformation for bimaterials with lower conversions at different strains: (a) 50% crosslinked; (b) 82% crosslinked. The different figures in each row represent strains (from left to right): (a) 56.6% and 98.1%; (b) 130% and 185.7%.

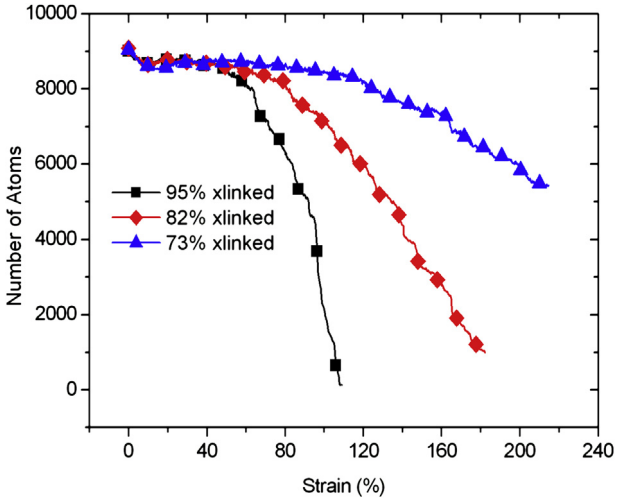

Fig. 14. Number of epoxy atoms within the van der Waals cutoff distance from the epoxy/Cu interface.

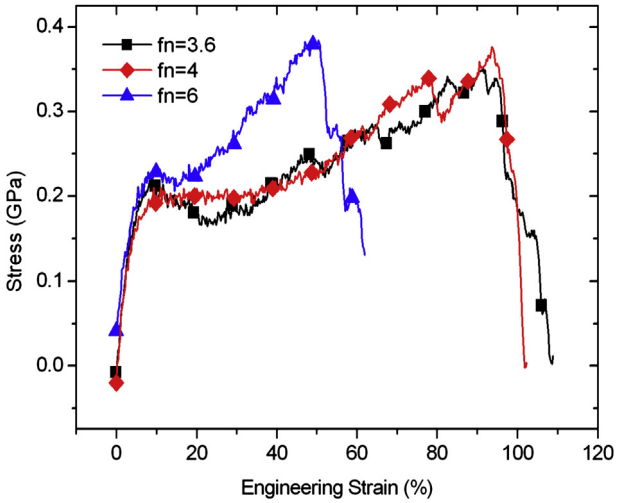

Fig. 15. Stress–strain curves for models with different epoxy monomer functionalities.

3.7. Effects of epoxy functionality

Results presented here so far are for the epoxy system containing tri- and tetra-functionalized epoxy monomers and the number-averaged functionality is 3.6. Different functionality results in different microstructure of the crosslinked polymer network. Therefore, it is conceivable that the mechanical behavior of the epoxy/Cu bimaterial would be different for epoxies with different functionalities. To study the effects of epoxy monomer functionality (fn) on the mechanical behavior of the epoxy/Cu bimaterial, two additional MD simulations were conducted on epoxy/Cu bimaterials with $fn = 4$ and 6, respectively. Fig. 15 plots the corresponding stress–strain curves together with that of $fn = 3.6$. Points of interest on the stress–strain curves are extracted and tabulated in Table 3.

Several observations regarding the change of fn from 3.6 to 6 can be made from Fig. 15 and Table 3. First, the yielding strength and yielding strain do not seem to change much, indicating that the bulk elastic properties are not sensitive to the epoxy functionality. Second, the failure strength does not seem to change much, indicating that interfacial strength is not sensitive to the epoxy functionality, since the failure strength of the bimaterial is decided by the epoxy/Cu interfacial strength. Third, although the interfacial strength does not change much, the failure strain of the bimaterial reduces significantly with increasing fn. Note that the post-yielding (between the yielding and failure) is a consequence of the changes in angular and torsional bonds, or the relative sliding between the polymer chains, reduction of the failure strength implies that angular and torsional bonds are more constrained in epoxy with higher functionality. This is intuitively understandable, because $fn = 6$ means that (on average) each epoxy monomer in the polymer network has six sites to bond to other epoxy monomers, resulted in a more closely inter-connected network which limits the chain sliding and local voiding. Consequently, bulk epoxy with higher functionality is less deformable. This can be observed from Fig. 16 where for $fn = 6$ the microstructure of the deformed epoxy/Cu bimaterial under different strain is shown. In comparison to Fig. 6 where the same is shown for $fn = 3.6$, it is clear that bulk epoxy with higher functionality has much less deformation, and much less and smaller voids.

4. Summary of conclusions

To investigate the deformation/failure behavior of epoxy/Cu interface, we carried out large scale classical molecular dynamics simulations on an epoxy/Cu bimaterial. The network structure of the epoxy was built through a simulated crosslinking process in which covalent bonds formation and MD equilibration of the system were performed iteratively. The crosslinked molecular network was applied on the Cu substrate to build the epoxy/Cu bimaterial. By applying velocity loading to the substrate on the fly of molecular dynamics simulations, the normal stress versus displacement/strain response was obtained. Effects of simulation cell size were studied to ensure that the results are independent of simulation cell size.

We found that normal stress versus strain curve exhibits a near linear elastic range, followed by yielding and post-yielding strain softening, and hardening regimes, ended with a brittle failure.

The deformation between yielding and ultimate failure of the epoxy/Cu bimaterial is predominately due to micro-void initiation/growth and re-alignment of the epoxy network strands. The ultimate failure is predominantly interfacial and brittle caused by the (almost) simultaneous detachment of epoxy atoms from the Cu substrate.

In addition, we found that the linear range of the stress–strain curve is almost unaffected by the conversion of the epoxy. However, epoxy with lower conversion tends to have lower failure strength, but large failure strain. This is because at lower

Table 2
Failure strengths and strains for bimaterials with different conversions.

Conversion (%)	Failure strength (GPa)	Failure strain (%)
50	0.2146	11.07
73	0.1470	170.48
82	0.2143	130.18
95	0.339	94.91

Table 3
Failure strengths and strains for different functionalities.

Functionality	Failure strength (GPa)	Failure strain (%)
3.6	0.339	94.91
4	0.376	93.78
6	0.384	50.45

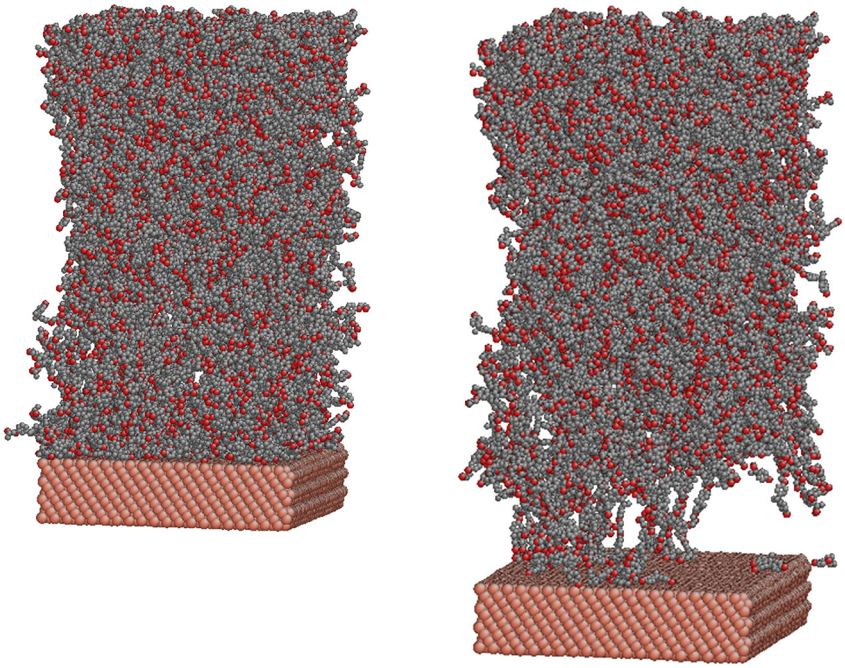

Fig. 16. Deformed atomistic configurations for the $fn = 6$ case. The different figures from left to right represent strains at 39.2% and 63.7%.

conversion, the polymer network is less connected, which facilitates void initiation and chain re-alignment leading to larger failure strain. The lower conversion also makes it easier for the epoxy atoms to be detached from the Cu substrate in a more gradual manner so that the ultimate interfacial failure becomes more ductile with a lower failure strength.

Further, the effects of epoxy functionality were also investigated. We found that epoxy with higher functionality tend to behave similarly to epoxy with higher conversion in that they are more brittle and have higher failure strength.

Another interesting finding is that the failure strength is unaffected by the unloading and reloading before the failure strength is reached, because the epoxy/Cu interface is not damaged until the stress is very close to the failure strength. This is more so for epoxy with higher conversion.

In closing, we point out that in interpreting the above results/conclusions, one must keep in mind the limitations of the classical molecular dynamics simulations, most notably, the small material volume simulated, and the high strain rate used. We believe that relatively high yielding strength of the epoxy, and the failure strength of the epoxy/Cu interface are partially due to these limitations. In spite of these limitations, we believe that major findings of this study provide significant insights into the deformation and failure of the epoxy/Cu bimaterial. The basic mechanisms captured by our MD simulation remain valid for laboratory-size samples under quasi-static loading.

Another concern is the infinite cohesive strength of the epoxy predicted by the PCFF force field used in the MD simulations. We note, however, that numerous experimental observations of epoxy adhesive on Cu substrate have shown that the epoxy/Cu interface is indeed the weakest link in the bimaterial system, unless special treatment is applied to the Cu surface before bonding. This is because the epoxy forms no chemical bonds with copper without any modification. Only weak van der Waals force and hydrogen bonds are involved in the adhesion [37]. Thus the Cu-epoxy interface has poor intrinsic adhesion and is prone to interfacial delamination instead of cohesive failure in the polymer. Therefore, it is reasonable to assume in our MD studies that interfacial failure occurs prior to bulk failure. Consequently, the cohesive strength of the bulk epoxy is not important as long as it is greater than the interfacial strength, since the stress in the bulk will never be high enough to reach the bulk strength. Thus, the use of PCFF is justified when interfacial failure is of the main interest.

Acknowledgments

The work was supported in part by a grant from NSF (CMMI-1200075).

References

[1] Lee HY. Materials Science and Engineering A – Structural Materials Properties Microstructure and Processing 2001;311(1–2):217–25.
[2] Lee HY, Qu JM. Journal of Adhesion Science and Technology 2003;17(2):195–215.
[3] Yu J, Song JY, Park IS. Journal of Electronic Materials 2002;31(12):1347–52.
[4] Gall K, Horstemeyer MF, Van Schilfgaarde M, Baskes MI. Journal of the Mechanics and Physics of Solids 2000;48(10):2183–212.
[5] Spearot DE, Jacob KI, McDowell DL. Mechanics of Materials 2004;36(9):825–47.
[6] Zhou XW, Moody NR, Jones RE, Zimmerman JA, Reedy ED. Acta Materialia 2009;57(16):4671–86.
[7] Zhou XW, Zimmerman JA, Reedy ED, Moody NR. Mechanics of Materials 2008;40(10):832–45.
[8] Bermejo JS, Ugarte CM. Macromolecular Theory and Simulations 2009;18(6):317–27.
[9] Doherty DC, Holmes BN, Leung P, Ross RB. Computational and Theoretical Polymer Science 1998;8(1–2):169–78.
[10] Komarov PV, Chiu YT, Chen SM, Khalatur PG, Reineker P. Macromolecules 2007;40(22):8104–13.
[11] Varshney V, Patnaik SS, Roy AK, Farmer BL. Macromolecules 2008;41(18):6837–42.
[12] Wu CF, Xu WJ. Polymer 2006;47(16):6004–9.
[13] Yang W, Wei DS, Jin XG, Liao Q. Macromolecular Theory and Simulations 2007;16(5):548–56.
[14] Yarovsky I, Evans E. Polymer 2002;43(3):963–9.
[15] Fan HB, Yuen MMF. Polymer 2007;48(7):2174–8.
[16] Tack JL, Ford DM. Journal of Molecular Graphics and Modelling 2008;26(8):1269–75.
[17] Yang SR, Qu JM. Polymer 2012;53(21):4806–17.
[18] Fan HB, Chan EKL, Wong CKY, Yuen MMF. Journal of Adhesion Science and Technology 2006;20(16):1937–47.
[19] Lin YC. Journal of Polymer Research 2006;13(5):369–74.

[20] Mijovic J, Zhang H. Journal of Physical Chemistry B 2004;108(8):2557–63.
[21] Yu S, Yang S, Cho M. Polymer 2009;50(3):945–52.
[22] Lorenz CD, Stevens MJ, Wool RP. Journal of Polymer Science Part B – Polymer Physics 2004;42(18):3333–43.
[23] Stevens MJ. Macromolecules 2001;34(8):2710–8.
[24] Tsige M, Stevens MJ. Macromolecules 2004;37(2):630–7.
[25] Mukherji D, Abrams CF. Physical Review E 2009;79(6):061802.
[26] Mukherji D, Abrams CF. Physical Chemistry Chemical Physics 2009;11(12):2113–5.
[27] Jia J, Huang YD, Long J, He JM, Zhang HX. Applied Surface Science 2009;255(13–14):6451–9.
[28] Cheng HC, Hsu YC, Wu CH, Chen WH. Applied Surface Science 2011;257(20):8665–74.
[29] Fan HB, Wong CKY, Yuen MMF, editors. IEEE 59th electronic components and technology conference 2009;vols. 1–4. p. 246–50.
[30] Jansen KMB. Structure of delft molding compound, (private communication).
[31] Material Studio, Accelrys Inc.
[32] Theodorou DN, Suter UW. Macromolecules 1985;18(7):1467–78.
[33] Hill JR, Sauer J. Journal of Physical Chemistry 1994;98(4):1238–44.
[34] Sun H. Journal of Computational Chemistry 1994;15(7):752–68.
[35] Sun H. Macromolecules 1995;28(3):701–12.
[36] Sun H, Mumby SJ, Maple JR, Hagler AT. Journal of the American Chemical Society 1994;116(7):2978–87.
[37] Wong CKY [PhD thesis]. The Hong Kong University of Science and Technology; 2008.
[38] Sun H. Journal of Physical Chemistry B 1998;102(38):7338–64.
[39] Plimpton S. Journal of Computational Physics 1995;117(1):1–19.
[40] Carlberger T, Alfredsson KS, Stigh U. International Journal for Computational Methods in Engineering Science and Mechanics 2008;9(5):288–99.
[41] Stigh U, Alfredsson KS, Andersson T, Biel A, Carlberger T, Salomonsson K. International Journal of Fracture 2010;165(2):149–62.
[42] Morgan RJ, O'Neal JE. Journal of Materials Science 1977;12(10):1966–80.
[43] Sue HJ, Bertram JL, Garciameitin EI, Puckett PM. Journal of Polymer Science Part B – Polymer Physics 1995;33(14):2003–17.
[44] Liu J, Sue HJ, Thompson ZJ, Bates FS, Dettloff M, Jacob G, et al. Macromolecules 2008;41(20):7616–24.
[45] Liu J, Sue HJ, Thompson ZJ, Bates FS, Dettloff M, Jacob G, et al. Acta Materialia 2009;57(9):2691–701.
[46] Swadener JG, Liechti KM, de Lozanne AL. Journal of the Mechanics and Physics of Solids 1999;47(2):223–58.
[47] Mello AW, Liechti KM. Journal of Applied Mechanics – Transactions of the Asme 2006;73(5):860–70.
[48] Ji GF, Ouyang ZY, Li GQ, Ibekwe S, Pang SS. International Journal of Solids and Structures 2010;47(18–19):2445–58.
[49] Marzi S, Biel A, Stigh U. International Journal of Adhesion and Adhesives 2011;31(8):840–50.
[50] Samuel AM, Samuel FH. Metallurgical and Materials Transactions A – Physical Metallurgy and Materials Science 1995;26(9):2359–72.
[51] Dighe MD, Gokhale AM. Scripta Materialia 1997;37(9):1435–40.
[52] Miller DR, Macosko CW. Macromolecules 1976;9(2):206–11.